Journal of Materials Chemistry A

Earth-abundant iron(III) species serves as a cocatalyst boosting the multi-electron reduction of IO_3^-/I^- redox shuttle in Z-scheme photocatalytic water splitting

Journal:	*Journal of Materials Chemistry A*
Manuscript ID	TA-ART-02-2021-001703.R1
Article Type:	Paper
Date Submitted by the Author:	08-Apr-2021
Complete List of Authors:	Murofushi, Katsuya; Kyoto University, Graduate School of Engineeing Ogawa, Kanta; Kyoto University, Graduate School of Engineering Suzuki, Hajime; Kyoto University, Graduate School of Engineering Sakamoto, Ryota; Kyoto University, Graduate School of Engineering Tomita, Osamu; Kyoto University, Graduate School of Engineering Kato, Kosaku; Toyota Technological Institute, Yamakata, Akira; Toyota Technological Institute, Graduate School of Enginnering Saeki, Akinori; Osaka University, Department of Applied Chemistry, Graduate School of Engineering Abe, Ryu; Kyoto University, Graduate School of Engineeing

ARTICLE

Earth-abundant iron(III) species serves as a cocatalyst boosting the multi-electron reduction of IO_3^-/I^- redox shuttle in Z-scheme photocatalytic water splitting

Received 00th January 20xx,
Accepted 00th January 20xx

DOI: 10.1039/x0xx00000x

Katsuya Murofushi,[a,†] Kanta Ogawa,[a,b,†] Hajime Suzuki,[a] Ryota Sakamoto,[a] Osamu Tomita,[a] Kosaku Kato,[c] Akira Yamakata,[c] Akinori Saeki,[d] Ryu Abe[a,b,*]

Z-scheme water splitting exhibits promising potential for practical water splitting under visible light irradiation. This system comprises two photocatalysts for O_2 and H_2 evolution and a redox shuttle couple for transporting electrons between these photocatalysts. Therefore, the promotion of the redox reaction of the shuttle is a crucial factor for efficient water splitting. In particular, for multielectron redox reactions (e.g. IO_3^-/I^-), cocatalyst is indispensable, where only noble metals may contribute thus far. Herein, we demonstrate that FeO_x catalyzes the reduction of multi-electron IO_3^- reduction on the Bi_4TaO_8Cl photocatalyst. While bare Bi_4TaO_8Cl does not show O_2 evolution from an aqueous IO_3^- solution because of the lack of multi-electron reduction ability, FeO_x loading enables O_2 evolution. Based on a series of experimental investigations, such as time-resolved spectroscopy, we elucidated that the O_2 evolution enhancement stems from the promotion of the multielectron reduction of IO_3^- by FeO_x. The Fe^{III}/Fe^{II} redox couple in the loaded FeO_x facilitates both electron carrier capture from Bi_4TaO_8Cl and reduction of the redox mediator. In addition, FeO_x is effective for other photocatalysts and redox mediators. In the present study, we developed the first earth-abundant cocatalyst for multielectron redox mediators.

Introduction

Water splitting based on semiconductor photocatalysts is regarded as a promising strategy to achieve clean hydrogen production from solar energy.[1–4] While several semiconductors, such as $SrTiO_3$, split water with high efficiencies under ultraviolet (UV) illumination,[4] visible light utilization is crucial for practical applications as nearly half of the solar energy incident on the earth lies in the visible light region. Z-scheme water splitting facilitates visible light utilization by allocating the Gibbs free energy for water splitting between two photocatalysts that are responsible for O_2 and H_2 evolution. Therefore, the two photocatalysts are tethered electrically by a redox shuttle couple (e.g., Fe^{3+}/Fe^{2+}, IO_3^-/I^-), which transports electrons between them.[1,5]

The IO_3^-/I^- couple has been employed as a redox shuttle in various Z-scheme systems,[5] enjoying an advantage that IO_3^-/I^- may work in mild pH conditions of 5 – 9, where most photocatalysts do not suffer from deactivation (e.g., dissolution).[6] However, its multi-electron reduction ($IO_3^- + 6H^+ + 6e^- \rightleftarrows I^- + 3H_2O$; 1.09 V vs. RHE) suffers from a small reaction rate on the O_2 evolution photocatalyst surface, which deteriorates the overall water splitting efficiency. Although facilitating this process should be crucial, cocatalysts for redox shuttles have attracted less attention than those for oxygen and hydrogen evolution reactions.[7] Thus far, the example of redox cocatalysts for IO_3^- is limited to noble metal species, such as Pt, Ru, and Ir,[6–11] leaving sufficient room for investigation, especially from the perspective of resources.

In this study, we demonstrate that earth-abundant iron oxide (FeO_x) functions as an effective cocatalyst for the 6-electron reduction of IO_3^-, allowing the Bi_4TaO_8Cl photocatalyst to evolve O_2 from water containing IO_3^-. A series of experimental investigations have argued that the Fe^{III}/Fe^{II} redox couple in FeO_x is responsible for the acceleration of electron capture from Bi_4TaO_8Cl and reduction of IO_3^-. FeO_x also serves as a redox cocatalyst for other photocatalysts and redox mediators. We also demonstrate that FeO_x-loaded Bi_4TaO_8Cl applies to a visible-light Z-scheme system with an IO_3^-/I^- redox shuttle.

Results and Discussion

Characterization of Fe species loaded on Bi_4TaO_8Cl

The FeO_x cocatalyst was loaded onto Bi_4TaO_8Cl via the impregnation method. The loading amount of the Fe species was set to be 10 mol% against Bi_4TaO_8Cl (approximately 0.5 wt% as Fe), unless otherwise stated. Negligible differences were

[a] Department of Energy and Hydrocarbon Chemistry, Graduate School of Engineering, Kyoto University, Nishikyo-ku, Kyoto 615-8510, Japan.
[b] AIST-Kyoto University Chemical Energy Materials Open Innovation Laboratory (ChEM-OIL), National Institute of Advanced Industrial Science and Technology (AIST), Sakyo-ku, Kyoto 606-8501, Japan.
[c] Graduate School of Engineering, Toyota Technological Institute, 2-12-1 Hisakata, Tempaku, Nagoya 468-8511, Japan
[d] Department of Applied Chemistry, Graduate School of Engineering, Osaka University, 2-1 Yamadaoka, Suita, Osaka 565-0871, Japan
†K.M. and K.O. contributed equally to this work
Electronic Supplementary Information (ESI) available: [XRD patterns, photocatalytic activity, Mott–Schottky analysis]. See DOI: 10.1039/x0xx00000x

observed in the XRD pattern and the band edge positions of Bi_4TaO_8Cl before and after the loading of FeO_x (Figs. S1 and S2). The FeO_x cocatalyst was identified by K-edge X-ray absorption near edge structure (XANES) spectroscopy (Fig. 1a). *β*-FeOOH, Fe_2O_3, $FeCl_3$, and FeO were used as the reference samples. $FeCl_3$ is the precursor for FeO_x loading. The FeO_x cocatalyst on Bi_4TaO_8Cl shows a spectrum similar to that of *β*-FeOOH and Fe_2O_3, while it exhibits a difference from that of FeO. This result demonstrates the trivalency of the loaded Fe species. As shown in Fig. 1b, we also acquired Fe K-edge Fourier-transformed extended X-ray absorption fine structure (EXAFS) spectra. *β*-FeOOH, Fe_2O_3, and $FeCl_3$ were used as the Fe (III) references. The FeO_x cocatalyst sample features a nearest neighbor distance similar to those for *β*-FeOOH and Fe_2O_3 while that for $FeCl_3$ is greater. Therefore, the nearest neighboring atom for Fe in the FeO_x cocatalyst is oxygen. From the XANES and EXAFS results, we conclude that the identity of FeO_x is trivalent oxides/oxyhydroxides. Transmission electron microscopy (TEM) revealed the amorphous nature of the FeO_x cocatalyst (Fig. 1c), which is highly dispersed on the photocatalyst (Fig. S3).

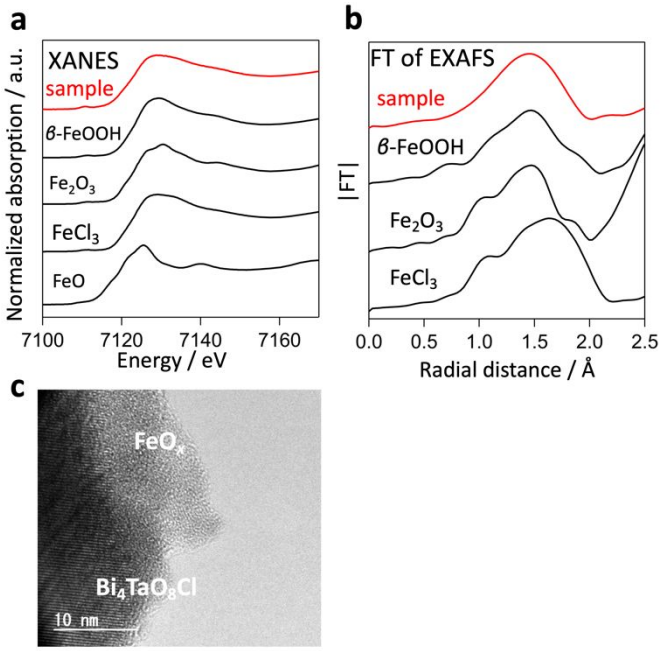

Fig. 1 Fe K-edge XANES (a) Fourier transforms of EXAFS (b) spectra for FeO_x-Bi_4TaO_8Cl. c, TEM image of FeO_x-Bi_4TaO_8Cl.

Activation of photocatalytic O_2 evolution by FeO_x

The photocatalytic activity of bare and FeO_x-loaded Bi_4TaO_8Cl for O_2 evolution was evaluated in the presence of IO_3^- as an electron acceptor. As shown in Fig. 2, bare Bi_4TaO_8Cl exhibited negligible O_2 evolution under visible-light irradiation (λ > 400 nm). Note that bare Bi_4TaO_8Cl is capable of oxidizing water into O_2 in the presence of one-electron acceptors ($Ag^+ + e^- \rightarrow Ag$; $Fe^{3+} + e^- \rightarrow Fe^{2+}$).[12,13] Therefore, the negligible activity of the bare sample should stem from the absence of active sites for the multielectron reduction of IO_3^-. In contrast, FeO_x-loaded Bi_4TaO_8Cl showed O_2 evolution at a relatively high and steady rate. The amount of evolved O_2 in 10 h was 65.6 µmol, which was much greater than the O_2 provided the stoichiometric oxidation of H_2O proceeded by loaded-FeO_x (17 µmol / 4 e^- = 4.2 µmol). Note that the loading amount and calcination temperature for FeO_x loading were optimized for the O_2 evolution reaction (Fig. S4) and the apparent quantum efficiency (AQE) at 420 nm was 1.4 %. The O_2 evolution of bare Bi_4TaO_8Cl was not improved by the addition of Fe^{3+} in the aqueous medium (Fig. S5), indicating that FeO_x loaded on the surface of the photocatalyst is essential for boosting O_2 evolution. The possibility of direct interfacial charge transfer[12] from the valence band maximum of Bi_4TaO_8Cl to Fe^{III} was ruled out by the negligible O_2 evolution under light irradiation below the band gap of Bi_4TaO_8Cl (Fig. S2). FeO_x-loaded and bare Bi_4TaO_8Cl did not show a significant difference in the pH-dependent zeta potentials (Fig. S6).

From these results, we concluded that FeO_x on Bi_4TaO_8Cl acts as a redox cocatalyst for the multielectron reduction of the IO_3^- electron acceptor. To the best of our knowledge, this is the first earth-abundant cocatalyst to promote IO_3^- reduction.

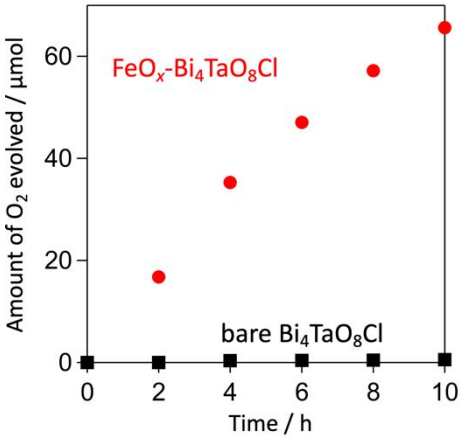

Fig. 2 Time courses of O_2 evolution over FeO_x-Bi_4TaO_8Cl (red circle) or bare Bi_4TaO_8Cl (black square) in aqueous $NaIO_3$ solution (4 mM) under visible-light (λ > 400 nm) irradiation.

Photogenerated electron capture by FeO_x

The role of a cocatalyst is to capture photogenerated carriers from the semiconductor photocatalyst and promote the catalytic reaction.[14] To clarify the electron capture ability of FeO_x, we employed time-resolved microwave conductivity (TRMC) measurement, which is known as a useful tool to investigate carrier dynamics in powdery photocatalysts.[15–17] Note that, based on the facts that the effective mass of electron is much smaller than that of holes in Bi_4TaO_8Cl (Fig. S7) and that the Bi_4TaO_8Cl is a n-type semiconductor, electrons mainly contribute to the TRMC signal of Bi_4TaO_8Cl. As shown in Fig. 3, FeO_x loading lowered the transient photoconductivity, which suggests efficient electron capture by FeO_x.

This assignment was further supported by time-resolved absorption spectroscopy (TRAS), another useful tool for examining carrier dynamics in semiconductor photocatalysts.[18] Fig. 4a shows microsecond transient absorption spectra for bare Bi_4TaO_8Cl, where the band gap excitation induces three absorption increases at 2,000 cm^{-1}, 13,800 cm^{-1}, and 21,400 cm^{-1} (Fig. 4a). Referring to previous results on TiO_2[19–23] and

$LaTiO_2N$,[18] the first is attributed to photogenerated free electrons in the conduction band (CB) and/or shallowly trapped electrons,[24,25] the second is attributed to the excitation of trapped electrons from the mid-gap state to the CB,[18] and the third to holes. We then acquired the initial decay profiles using femtosecond TRAS, focusing on 2,000 cm^{-1} and 21,400 cm^{-1}. Fig. 4b and c show the decay curves of the bare Bi_4TaO_8Cl and FeO_x-Bi_4TaO_8Cl. The loading of FeO_x accelerated the decay of free electrons (Fig. 4b) while the influence on the hole decay was found to be negligible (Fig. 4c). These results indicate that FeO_x selectively captured electrons from Bi_4TaO_8Cl.

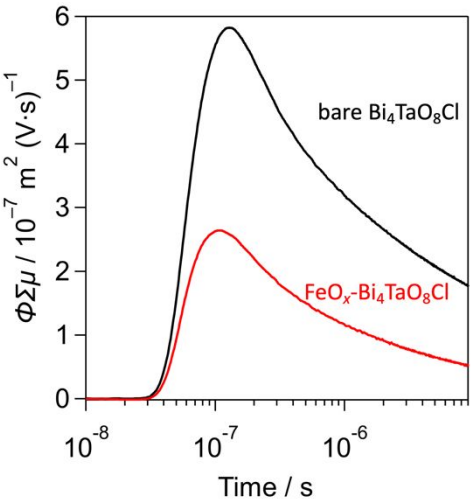

Fig. 3 TRMC transients of FeO_x loaded (red) or bare (black) Bi_4TaO_8Cl samples (λ_{ex} = 355 nm, $I_0 = 4.6 \times 10^{15}$ photons cm^{-2} $pulse^{-1}$).

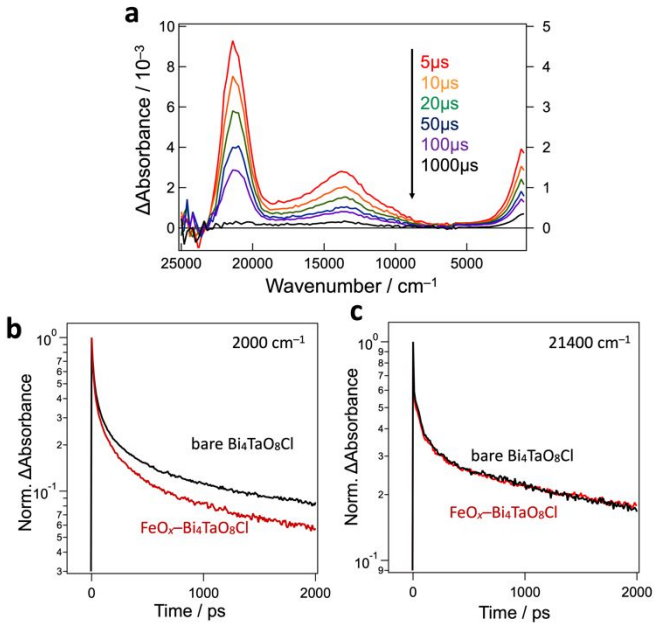

Fig. 4 a, Microsecond TRAS of bare Bi_4TaO_8Cl measured in the vacuum. The sample was excited by 355 nm laser pulses (6 ns duration, 0.5 mJ, 5 Hz). b, c, Femtosecond decay profiles of transient absorptions at 2,000 cm^{-1} (b) and 21,400 cm^{-1} (c) for bare Bi_4TaO_8Cl, FeO_x-Bi_4TaO_8Cl. The samples were excited by 355 nm laser pulses (90 fs duration, 6 μJ, 500 Hz) under air for the several pico-second (ps) region.

The catalytic property of FeO_x for IO_3^- reduction

To verify the catalytic activity of FeO_x for the reduction of IO_3^-, an FeO_x-decorated electrode was prepared on a fluorine-doped tin oxide (FTO) glass plate. Fig. 5 shows the cyclic voltammograms obtained using bare FTO and the FeO_x/FTO electrodes. In the absence of the IO_3^-, the FeO_x/FTO electrode exhibited a small cathodic current at approximately −0.0 ~ −0.3 V vs. Ag/AgCl; through referral to a previous report on a FeOOH electrode,[26] this was attributed to the reduction of Fe^{III} to Fe^{II}. The presence of IO_3^- did not affect the onset potential of cathodic current from Fe^{III} reduction (observed from about 0.0 V), which was followed by intense cathodic currents with an onset potential of approximately −0.4 V. The second cathodic current may stem from the catalytic reduction of IO_3^- by the produced Fe^{II} species, because, in the absence of FeO_x (bare-FTO), the cathodic current was much lower. In addition, the anodic current from Fe^{II} oxidation (observed from approximately −0.7 to −0.2 V) was suppressed by the increased IO_3^- concentration. This result also suggests that the produced Fe^{II} species during the cathodic sweep were consumed for IO_3^- reduction.

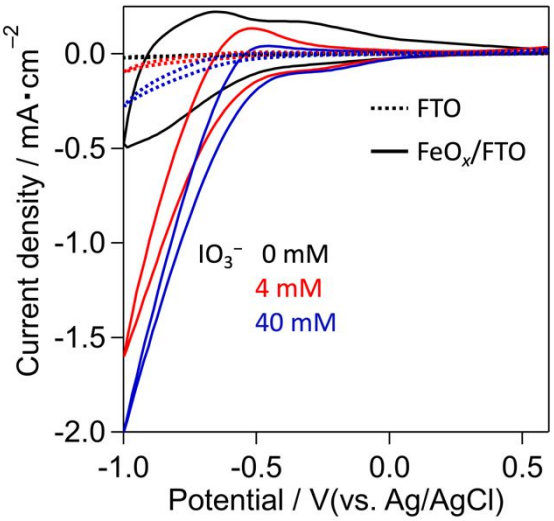

Fig. 5 Cyclic voltammogram of a FeO_x/FTO and FTO electrode in 0.1 M Na_2SO_4 solution containing 0–40 mM IO_3^- (pH 5), at a scan rate of 50 mVs^{-1}

The working mechanism of FeO_x cocatalyst

Based on the above-mentioned results, the role of FeO_x as a cocatalyst for IO_3^- reduction is illustrated in Fig. 6. After photoexcitation of the Bi_4TaO_8Cl photocatalyst, photogenerated electrons in the conduction band are captured by FeO_x (step 1). As a result, Fe^{III} is reduced to Fe^{II} (step 2), which allows FeO_x to accumulate electrons. Then, Fe^{II} ions reduce IO_3^- to I^- while Fe^{II} is re-oxidized to Fe^{III} (step 3). Through the catalytic cycle (steps 1 – 3), FeO_x can facilitate both carrier capture from the photocatalyst and reduction of the redox mediator, functioning as a cocatalyst. Step 1 was confirmed by time-resolved spectroscopy (Figs. 3 and 4). Step 3 was proposed using electrochemical measurements (Fig. 5).

Although we have not yet achieved direct observation of the Fe^{II} species generated in FeO_x (step 2) (Fig. S8), the generation of Fe^{II} was indirectly confirmed. Based on the Pourbaix diagram,[27] Fe^{II} species should dissolve in the aqueous solution as Fe^{2+} when the pH is approximately 5. Actually, visible light irradiation (10 h) on FeO_x-Bi_4TaO_8Cl in an aqueous solution without IO_3^- produced Fe^{2+} in the aqueous phase, as detected by a colorimetric method (Fig. S9). The amount of the produced Fe^{2+} (6.1 μmol) was approximately 36 % of the initial Fe^{III} species (17 μmol) within the loaded FeO_x. The production of Fe^{2+} should be accompanied by O_2 evolution, but the produced amount of the O_2 (2.1 μmol) was about 38% more than the estimated amount (1.5 μmol) from the Fe^{2+} detected in the aqueous solution (6.1 μmol), which in turn implies that a part of produced Fe^{II} remains in the FeO_x without dissolving in water. In sharp contrast, the presence of IO_3^- suppressed the dissolution of FeO_x during the O_2 evolution reaction (Fig. S9), which suggests that the Fe^{II} species produced in FeO_x were promptly re-oxidized to insoluble Fe^{III} in the photocatalytic reaction by IO_3^-. Despite the persistency of the Fe^{II} species on Bi_4TaO_8Cl in the presence of IO_3^-, the stability of the O_2 evolution has still large room to improve, which results from, for example, the aggregation and surface passivation of FeO_x on Bi_4TaO_8Cl (Fig. S10).

Steps 2 and 3 were further verified by a complementary experiment, in which the spontaneous reduction of IO_3^- by Fe^{II} (Eq. (1)) were tested (Fig. S11).

$$IO_3^- + 6Fe^{II} + 6H^+ \longrightarrow I^- + 6Fe^{III} + 3H_2O \quad (1)$$

An $Fe(OH)_2$ colloidal solution (greenish-white, as shown in Fig. S11a) was added to an aqueous solution of $NaIO_3$. After mixing, the color of the solution changed immediately to brown, indicating the formation of $Fe(OH)_3$ (Fig. S11d). In contrast, the addition of $Fe(OH)_2$ to pure water resulted in no color change (Fig. S11e). Fig. 7 shows the time courses of the Fe^{II} amounts in each mixture, which were quantified by colorimeter analysis (see the details in the experimental section). Fe^{II} was rapidly consumed to reduce IO_3^-. Another important finding was the almost complete (i.e., via 6-electrons) reduction of IO_3^- to I^-, without leaving other intermediates, such as I_2 (or I_3^-); this was confirmed by the quantification of IO_3^- and I^- through ion chromatography. As summarized in Table 1, the amounts of Fe^{II}, IO_3^-, and I^- were roughly in accordance with the theoretical amount from Eq. (1).

The above results and discussion emphasize the proposed role of FeO_x as a cocatalyst to boost O_2 evolution on the Bi_4TaO_8Cl photocatalyst with an IO_3^- electron acceptor (Fig. 6). Although the actual redox potential of Fe^{III}/Fe^{II} in FeO_x remains elusive, based on the redox potentials of Fe species (e.g., $Fe(OH)_3/Fe(OH)_2$: −0.02 V; $Fe(OH)_3/Fe^{2+}$: +0.17 V vs. SHE at pH 5) and IO_3^- (IO_3^-/I^-: +0.79 V vs. SHE at pH 5), Fe^{II} can thermodynamically reduce IO_3^-. Further application of the present FeO_x cocatalyst to various semiconductors may shed light on the redox potential, as will be discussed in the next section.

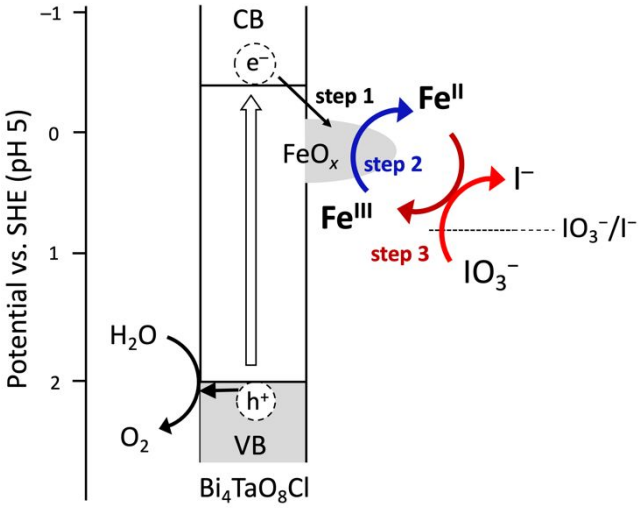

Fig. 6 Schematic illustration of the role of FeO_x deposited on the photocatalyst to promote reduction of IO_3^-.

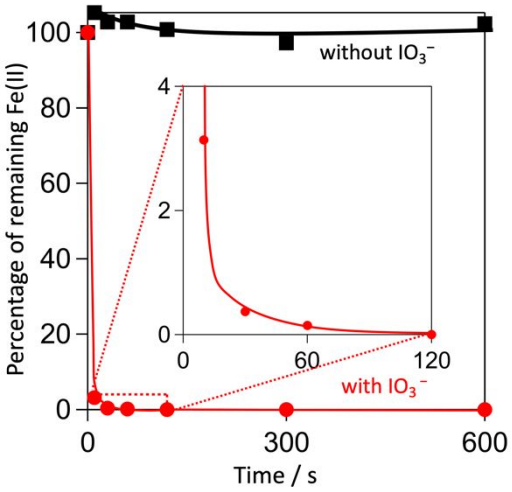

Fig. 7 Time course of the Fe(II) amount after the adding of $Fe(OH)_2$ colloidal solution to IO_3^- aqueous solution (red) and water (black).

Table 1 The amount (μmol) of reactants in the IO_3^- solution after adding the $Fe(OH)_2$ colloidal solution

	before	After 10 min	Estimated amount from Eq. (1).
IO_3^-	400 μmol	355	333
I^-	0	61	67
Fe(II)	400	n.d.	0

Applicability to other photocatalysts and redox

We investigated the utility of FeO_x in other photocatalysts and redox shuttles. FeO_x was found to be effective for other

photocatalysts, improving the O_2 evolution activity of $BiVO_4$ and anatase-TiO_2 in the presence of the IO_3^- electron acceptor (Table 2). In contrast, it did not work for WO_3. The effect of FeO_x reliant on photocatalysts is in stark contrast to previous cocatalysts for IO_3^- reduction (e.g., Pt is effective for both $BiVO_4$ and WO_3),[1] providing a hint on the redox potential of Fe^{III}/Fe^{II} in FeO_x. It is widely recognized that the conduction band minimum of WO_3 is more positive than that of $BiVO_4$.[28] We also measured the flatband potentials of $BiVO_4$ and WO_3 as −0.10 and +0.04 V (vs. SHE at pH 5), respectively (Fig. S12). Thus, the lack of enhancement of WO_3 by FeO_x strongly suggests the insufficient reduction power of photoexcited electrons in WO_3 for Fe^{III}/Fe^{II} in FeO_x.

It is noteworthy that FeO_x loading on Bi_4TaO_8Cl is also effective for other redox mediators (not only multi-electron acceptors), such as $Co^{III}(bpy)_3^{3+}$ or $Fe(CN)_6^{3-}$ (Table 2). In each case, the evolved O_2 is more significant than the estimated O_2 evolution, accompanied by the reduction in all the loaded-FeO_x (Fe^{III}) to Fe^{II} (4.2 μmol). These results also indicate that the redox potential of Fe^{III}/Fe^{II} in FeO_x is more negative than those of $Co^{III}(bpy)_3^{3+}$ (+0.32 V) and $Fe(CN)_6^{3-}$ (+0.37 V). Given the above, the redox potential of Fe^{III}/Fe^{II} in FeO_x seems to be located between −0.10 and +0.32 V (vs. SHE at pH 5).

The Pourbaix diagram for Fe species[27] provides us the redox of $Fe(OH)_3/Fe^{2+}$ (+0.17 V) when pH is 5. However, this potential should not directly apply to the present situation where Fe^{II} is in FeO_x not in the solution. We may estimate the redox potential of Fe^{III}/Fe^{II} in FeO_x from another related redox: $Fe(OH)_3/Fe(OH)_2$ existing only above pH 9 from the Pourbaix diagram. Assuming that Fe^{II} does not dissolve into water even at pH 5, and that the redox of $Fe(OH)_3/Fe(OH)_2$ follows a Nernst slope, the redox potential might be approximately −0.02 V (vs. SHE at pH 5). This hypothetical value falls within the above-mentioned value (−0.10 ~ +0.32 V) and might justify the Fe^{III}/Fe^{II} redox cycles with hydroxide forms in FeO_x (Fig. 6). Although further studies are necessary, these results suggest that FeO_x loading can apply to other redox-based photocatalytic O_2 evolution systems if the potential relationship is appropriate (i.e., conduction band < Fe^{III}/Fe^{II} < electron acceptor).

Table 2 The effect of FeO_x loading on O_2 evolution reaction

Photocatalyst	Electron Acceptor	O_2 evolution in 3h / μmol	
		bare	with FeO_x
$BiVO_4$	IO_3^-	12.7	28.5
TiO_2	IO_3^-	7.3	28.3
WO_3	IO_3^-	n.d.	<0.2
Bi_4TaO_8Cl	$Co^{III}(bpy)_3^{3+}$	5.1	70.3
Bi_4TaO_8Cl	$Fe(CN)_6^{3-}$	n.d.	57.4

Z-scheme water splitting

Finally, we applied FeO_x-loaded Bi_4TaO_8Cl to a Z-scheme water splitting system as an O_2 evolution photocatalyst. Herein, the IO_3^-/I^- couple as a redox mediator and Pt-loaded strontium titanate doped with Rh cations[29] (Pt/$SrTiO_3$:Rh) as a H_2-evolving photocatalyst were employed. As shown in Fig. 8, H_2 and O_2 evolved stoichiometrically upon illumination with λ > 400 nm light, demonstrating visible-light Z-scheme water splitting.

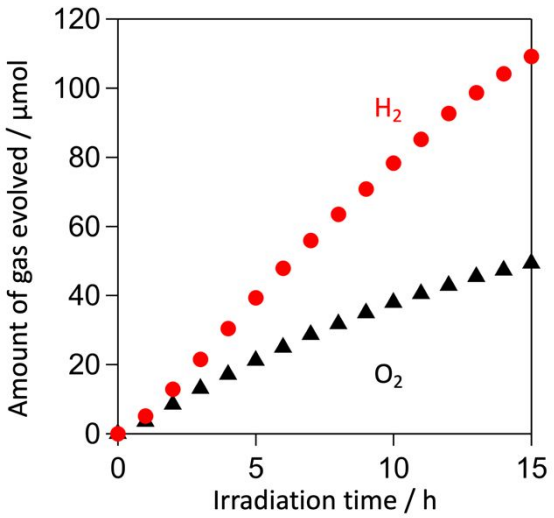

Fig. 8 Time course of H_2 and O_2 evolution over a mixture of FeO_x-Bi_4TaO_8Cl sample (50 mg) and Pt/$SrTiO_3$:Rh (100 mg) in NaI (0.98 mM) and $NaIO_3$ (0.02 mM) aqueous solution (250 mL) at pH 5 under visible light irradiation (λ > 400 nm)

Conclusions

In this study, we demonstrated that FeO_x catalyzes the reduction of multi-electron IO_3^- on the surface of photocatalysts. Based on experimental investigations, such as time-resolved spectroscopy, we elucidated the mechanism of the IO_3^- reduction by FeO_x. The redox cycle of (Fe^{III}/Fe^{II}) in the loaded FeO_x facilitates both the carrier capture from the photocatalyst and the reduction of the redox mediator. In addition, the loading of FeO_x was effective for other photocatalysts and redox mediators. We believe that the present strategy, modification by FeO_x promoting photocatalytic reactions via its redox cycle (Fe^{III}/Fe^{II}), can be widely applied to other photocatalytic systems and other transition metal species. Moreover, various materials containing transition metal cations with tunable redox potentials, such as hexacyanoferrate-based materials[30] and metal-organic frameworks[31], are potential candidates for such cocatalysts. The present study marks the dawn of earth-abundant cocatalysts applicable to various redox mediators, paving the way for the future of visible-light water splitting.

Experimental section

Synthesis

Bi_4TaO_8Cl was prepared by a two-step synthesis via the polymerized complex (PC) method according to the literature.[13] The particulate Bi_3TaO_7 sample was initially prepared by the PC method as follows: $Bi(NO_3)_3 \cdot 5H_2O$ (9 mmol, FUJIFILM Wako

Pure Chemical Corporation) and $TaCl_5$ (3 mmol, Kojundo Chemical Laboratory Co., Ltd.) were mixed in methanol (20 mL) followed by addition of citric acid (0.13 mol, FUJIFILM Wako Pure Chemical Corporation). The mixture was stirred at 423 K to obtain a transparent solution. After the addition of ethylene glycol (32 mL, FUJIFILM Wako Pure Chemical Corporation), the solution was heated at 593 K on a hot stirrer with stirring. The obtained brown gel was further heated at 623 K using a mantle heater to produce a black solid mass. Finally, the black solid mass was calcinated at 773 K for 2 h in air. The produced Bi_3TaO_7 (6.7 mmol) was then mixed with BiOCl (FUJIFILM Wako Pure Chemical Corporation, 7.0 mmol), followed by heating in an evacuated silica tube at 973 K for 20 h.

$SrTiO_3$:Rh was prepared by solid-state reaction.[32] A mixture of TiO_2, $SrCO_3$ and Rh_2O_3 (Ti : Sr : Rh = 1 : 1.07 : 0.01) was calcined in air at 1073 K for 1 h and subsequently at 1273 K for 10 h. A Pt cocatalyst (0.5 wt% calculated as metal) was loaded onto $SrTiO_3$:Rh by the impregnation method using $H_2PtCl_6{\cdot}6H_2O$ (FUJIFILM Wako Pure Chemical Corporation) as a precursor by calcination at 473 K for 1 h in H_2 flow (20 mLmin^{-1}). $BiVO_4$ was prepared according to literature via a room temperature aqueous process.[33] A commercially available WO_3 (Kojundo Chemical Laboratory Co., Ltd., consisting mainly of monoclinic as well as a portion of triclinic phase) was used after the removal of the fine particles with triclinic phase by several cycles of an ultrasonic dispersion into Milli-Q water followed by centrifugation at 1000 rpm for 10 min.[34] A commercially available TiO_2 (Merck, Anatase) was used. *б*-FeOOH was also synthesized according to the literature[35] for a reference sample in the X-ray absorption experiments.

Deposition of FeO_x

The Fe species were loaded using the impregnation method. The Bi_4TaO_8Cl powder (0.3 g) was dispersed in an aqueous solution containing $FeCl_3$ (12.75 mM, 2.0 mL) followed by evaporation of the solvent in a water bath, and heat treatment at 573 K for 1 h in an Ar flow (20 mLmin^{-1}). The loading amount of Fe species was set to 10 mol% for the Bi_4TaO_8Cl.

Characterization

Powder XRD (MiniFlex II, Rigaku, X-ray source: Cu Kα), UV-visible diffuse reflectance spectroscopy (V-650, JASCO), SEM-EDX (NVision 40, Carl Zeiss-SIINT) were used to characterize the samples. Transmission electron microscopy (TEM) was performed using a JEOL JEM-2100F microscope. Fe K-edge X-ray absorption fine structure (XAFS) measurements were performed at the BL01B1 beamline of SPring-8. The X-ray absorption spectra were measured in transmission or fluorescence mode at room temperature using a Si(111) two-crystal monochromator.

Photocatalytic reaction

Photocatalytic reactions were performed using a gas closed-circulation system. Photocatalyst powders (0.2 g) were dispersed in an aqueous $NaIO_3$ solution (4 mM, 250 mL) in a Pyrex cell. The photocatalysts were irradiated with visible light (λ > 400 nm) through a cutoff filter (HOYA; L42) from a 300-W Xe-arc lamp (PerkinElmer; Cermax- PE300BF). In the case of TiO_2, UV and visible light were irradiated without the cutoff filter (λ > 300 nm). The quantity of the evolved gases was determined using an online gas chromatograph (thermal conductivity detector; molecular sieve 5 Å column packing; Ar carrier gas). The apparent quantum efficiency (AQE) for O_2 evolution was measured using a Xe lamp (MAX-302, Asahi Spectra Co. Ltd.) attached with a bandpass filter (central wavelength: 420 nm).

The Z-scheme water-splitting reaction was conducted using FeO_x-loaded Bi_4TaO_8Cl (50 mg) and Pt-loaded $SrTiO_3$:Rh (100 mg) as O_2- and H_2-evolving photocatalysts, respectively. They were suspended in NaI (0.98 mM) and $NaIO_3$ (0.02 mM) aqueous solution (250 mL) at pH 5. The suspension was irradiated with visible light (λ > 400 nm).

Electrochemical experiment

The FeO_x electrode was prepared by the drop-casting method on a fluorine-doped tin oxide (FTO) glass electrode. A small amount (50 μL) of $FeCl_3$ MeOH solution (12.5 mM) was spread on an FTO substrate. The substrate was dried in air at room temperature and subsequently calcined under an Ar flow (20 mL min^{-1}) at 573 K for 1 h. Electrochemical measurements were performed using a potentiostat (VersaSTAT4, Princeton Applied Research Co., Ltd.) and a cell consisting of a prepared electrode, Pt wire, and Ag/AgCl electrode as the working electrode, counter electrode, and the reference electrode, respectively.

Mott–Schottky measurements were conducted to evaluate the flat-band potential of semiconductors as follows: The sample was mixed with a small amount of water, and the obtained paste was coated on a fluorine-doped tin oxide (FTO) conductive substrate via a squeezing method and dried in air at 80 °C. The Mott–Schottky plots were recorded using electrochemical analyzer (PARSTAT2263, Princeton Applied Research). Electrochemical measurements were performed in a three-electrode cell and a Na_2SO_4 solution (0.5 M, pH 5.0 adjusted by HCl) with 10 mV amplitude and a frequency of 1 kHz. The flat-band potentials are assumed to be CBMs owing to the n-type nature of the samples.

Reaction between $Fe(OH)_2$ and IO_3^-

All the experiments were conducted under Ar bubbling to prevent the oxidation of Fe^{II} by O_2 in air. $Fe(OH)_2$ colloidal solution (0.2 M as Fe, greenish-white) was prepared as described in the literature.[36] First, $FeCl_2 \cdot 4H_2O$ (10 mmol) was dissolved in Milli-Q water (30 mL). Then, the $FeCl_2$ aq. (0.33 M, 30 mL) was mixed with aqueous NaOH (1 M, 20 mL) with vigorous stirring. 2 mL of this colloidal solution was added to the aqueous solution with or without $NaIO_3$ (4 mM, 100 mL, adjusted to pH5 using HCl aq.) with stirring.

After stirring the mixed solutions, 500 μL of each solution was sampled and immediately added to aqueous HCl (1 M, 4.5 mL). The obtained solution (50 μL), 2 M acetate buffer solution (2.1 mL), and 9.6×10^{-4} M TPTZ solution (0.7 mL) were mixed, and the

amount of Fe^{2+} was determined based on the absorbance at 596.5 nm using UV-vis spectroscopy (UV-1800, Shimadzu).

For quantification of IO_3^- and I^-, 500 μL of this mixed solution was sampled and added to Milli-Q water (4.5 mL). Then, IO_3^- and I^- in the solution were quantified by ion chromatography (CDD-10ASP, Shim-pack, IC-SA2, Shimadzu).

TRMC Measurement

An X-band microwave (~9.1 GHz) was used as the probe. The third harmonic generation (THG; 355 nm) of a Nd:YAG laser (Continuum Inc., Surelite II, 5–8 ns pulse duration, 10 Hz) as the excitation source (4.6×10^{15} photons cm^{-2} $pulse^{-1}$) The powdered samples were fixed to quartz substrates using optically clear adhesive tape (the tape does not interfere with any TRMC signal). The photoconductivity $\Delta\sigma$ was calculated using the following formula: $\Delta\sigma = \Delta P_r/(AP_r)$, where ΔP_r, A, and P_r are the transient power change of the reflected microwave, the sensitivity factor, and the power of microwave reflected, respectively. The obtained $\Delta\sigma$ values were then converted to the product of the quantum yield (φ) and the sum of the charge carrier mobilities ($\sum\mu = \mu_+ + \mu_-$) using the following formula: $\varphi \sum\mu = \Delta\sigma(eI_0F_{light})^{-1}$, where e and F_{light} are the unit charge of a single electron and a correction (or filling) factor, respectively. All TRMC measurements were performed in an ambient atmosphere at room temperature (25°C).

TRAS measurement

A set of custom-built TRAS spectrometers was employed as described previously.[18] In the femtosecond to nanosecond regions, experiments were performed using a conventional pump–probe method based on a Ti:sapphire laser system (Spectra Physics, Solstice & TOPAS Prime; duration, 90 fs; repetition rate, 1 kHz). In this experiment, a 355 nm laser pulse was used as the pump pulse. The experiments were performed in air to prevent heating of the sample and to minimize the accumulation of electrons in the photocatalyst due to the high-frequency pump pulse irradiation (500 Hz). In the microsecond to second region, the transient absorption spectra were measured from 25,000 to 1,000 cm^{-1}. A 355 nm light (Continuum, Surelite-II, 6 ns, 355 nm, repetition rate of 5–0.01 Hz) was used as the pump pulse. The spectra were obtained at intervals of 200 cm^{-1} and averaged over 300 scans per spectrum. The measurements were performed under vacuum at room temperature. The powder photocatalyst was fixed on a CaF_2 plate with a density of ~1 mg cm^{-2}, and the obtained sample plate was placed in a stainless steel cell.

Density Functional Theory Calculation

The band structure calculation of Bi_4TaO_8Cl was performed within the framework of density functional theory (DFT) using a plane-wave pseudopotential method as implemented in the Cambridge Serial Total Energy Package (CASTEP) code of BIOVIA's Material Studio 2020.[37] The Perdew-Burke-Ernzerhof (PBE) function of the generalized gradient approximation (GGA) was employed as the exchange-correlation functional. A plane wave basis set with an energy cut-off of 630 eV and the Monkhorst-Pack 3 × 3 × 1 k-point mesh was used. The minimization algorithm of Broyden–Fletcher–Goldfarb–Shanno (BFGS) was employed for geometry optimizations with a total energy convergence tolerance of 10^{-6} eV per atom. The separation between the k-points in the band structure calculations was 0.001 Å. Other convergence parameters are as follows: a self-consistent field tolerance of 1×10^{-5} eV per atom, a maximum stress of 0.05 GPa, and the maximum ionic displacement of 1×10^{-3} Å.

The effective mass m* was calculated based on the obtained band structure. m* is defined as follows.

$$\frac{m_0}{m^*} = \frac{m_0 d^2\varepsilon}{\hbar^2 dk^2} \quad (2)$$

where m_0 is the free electron mass, k is the reciprocal lattice vector in the direction of interest, and $d^2\varepsilon/dk^2$ is the curvature of the band at a maximum or minimum, respectively. Assuming the band around their minima/maxima to be parabolic, we estimate the curvature of the band using the finite difference approximation:

$$\frac{d^2\varepsilon}{dk^2} \approx \frac{2[\varepsilon(k+\Delta k)-\varepsilon(k)]}{\Delta k^2} \quad (3)$$

where Δk = 0.05 Å.

Author Contributions

Katsuya Murofushi: Data curation, investigation, methodology visualization, writing–original draft. Kanta Ogawa: conceptualization, investigation, methodology, writing–original draft. Hajime Suzuki: writing–review & editing. Ryota Sakamoto: conceptualization, writing–review &editing. Osamu Tomita: investigation. Kosaku Kato: investigation. Akira Yamakata: resources, data curation. Akinori Saeki: resources, data curation. Ryu Abe: resources, supervision, writing–review &editing.

Conflicts of interest

There are no conflicts to declare.

Acknowledgements

This work was financially supported by the JST-CREST project, the JSPS KAKENHI Grant Number 17H06439 in Scientific Research on Innovative Areas "Innovations for Light-Energy Conversion (I4LEC)" and the JSPS Research Fellow (Grant Number 19J23357). This work was also supported by the Iketani Science and Technology Foundation and the TEPCO Memorial Foundation. The X-ray absorption experiments were performed at the BL01B1 beamline with the approval of the Japan Synchrotron Radiation Research Institute (JASRI) (Proposal No. 2019B1394). We are grateful to Dr. Saburo Hosokawa of Kyoto University for his helpful support in XAFS analysis. We also acknowledge financial support from AIST.

Notes and references

1 R. Abe, *BCSJ*, 2011, **84**, 1000–1030.
2 M. R. Shaner, H. A. Atwater, N. S. Lewis and E. W. McFarland, *Energy Environ. Sci.*, 2016, **9**, 2354–2371.
3 R. Bala Chandran, S. Breen, Y. Shao, S. Ardo and A. Z. Weber, *Energy Environ. Sci.*, 2018, **11**, 115–135.
4 T. Takata, J. Jiang, Y. Sakata, M. Nakabayashi, N. Shibata, V. Nandal, K. Seki, T. Hisatomi and K. Domen, *Nature*, 2020, **581**, 411–414.
5 B. Ng, L. K. Putri, X. Y. Kong, Y. W. Teh, P. Pasbakhsh and S. Chai, *Adv. Sci.*, 2020, **7**, 1903171.
6 Y. Miseki, S. Fujiyoshi, T. Gunji and K. Sayama, *Catal. Sci. Technol.*, 2013, **3**, 1750.
7 Y. Iwase, O. Tomita, M. Higashi, A. Nakada and R. Abe, *Sustainable Energy Fuels*, 2019, **3**, 1501–1508.
8 H. Suzuki, S. Nitta, O. Tomita, M. Higashi and R. Abe, *ACS Catal.*, 2017, **7**, 4336–4343.
9 M. Tabata, K. Maeda, M. Higashi, D. Lu, T. Takata, R. Abe and K. Domen, *Langmuir*, 2010, **26**, 9161–9165.
10 K. Maeda, R. Abe and K. Domen, *J. Phys. Chem. C*, 2011, **115**, 3057–3064.
11 M. Higashi, R. Abe, A. Ishikawa, T. Takata, B. Ohtani and K. Domen, *Chem. Lett.*, 2008, **37**, 138–139.
12 H. Kunioku, A. Nakada, M. Higashi, O. Tomita, H. Kageyama and R. Abe, *Sustainable Energy Fuels*, 2018, **2**, 1474–1480.
13 A. Nakada, A. Saeki, M. Higashi, H. Kageyama and R. Abe, *J. Mater. Chem. A*, 2018, **6**, 10909–10917.
14 K. Maeda and K. Domen, *BCSJ*, 2016, **89**, 627–648.
15 K. Ogawa, A. Nakada, H. Suzuki, O. Tomita, M. Higashi, A. Saeki, H. Kageyama and R. Abe, *ACS Appl. Mater. Interfaces*, 2019, **11**, 5642–5650.
16 A. Saeki, S. Yoshikawa, M. Tsuji, Y. Koizumi, M. Ide, C. Vijayakumar and S. Seki, *J. Am. Chem. Soc.*, 2012, **134**, 19035–19042.
17 H. Suzuki, S. Kanno, M. Hada, R. Abe and A. Saeki, *Chem. Mater.*, 2020, **32**, 4166–4173.
18 A. Yamakata, M. Kawaguchi, N. Nishimura, T. Minegishi, J. Kubota and K. Domen, *J. Phys. Chem. C*, 2014, **118**, 23897–23906.
19 B. H. Meekins and P. V. Kamat, *J. Phys. Chem. Lett.*, 2011, **2**, 2304–2310.
20 D. Bahnemann, A. Henglein, J. Lilie and L. Spanhel, *J. Phys. Chem.*, 1984, **88**, 709–711.
21 D. W. Bahnemann, M. Hilgendorff and R. Memming, *J. Phys. Chem. B*, 1997, **101**, 4265–4275.
22 T. Yoshihara, R. Katoh, A. Furube, Y. Tamaki, M. Murai, K. Hara, S. Murata, H. Arakawa and M. Tachiya, *J. Phys. Chem. B*, 2004, **108**, 3817–3823.
23 Y. Tamaki, A. Furube, M. Murai, K. Hara, R. Katoh and M. Tachiya, *J. Am. Chem. Soc.*, 2006, **128**, 416–417.
24 J. I. Pankove, *Optical Processes in Semiconductors*, New York, Dover Publication, 1975.
25 P. K. Basu, *Theory of Optical Processes in Semiconductors*, Oxford University Press, New York, 1997.
26 M. Fracchia, A. Visibile, E. Ahlberg, A. Vertova, A. Minguzzi, P. Ghigna and S. Rondinini, *ACS Appl. Energy Mater.*, 2018, **1**, 1716–1725.
27 M. Pourbaix, *Atlas of electrochemical equilibria in aqueous solutions*, National Association of Corrosion Engineers, Houston, Texas, USA, 1974.
28 S. J. Hong, S. Lee, J. S. Jang and J. S. Lee, *Energy Environ. Sci.*, 2011, **4**, 1781.
29 29 Y. Sasaki, A. Iwase, H. Kato and A. Kudo, *Journal of Catalysis*, 2008, **259**, 133–137.
30 30 A. Paolella, C. Faure, V. Timoshevskii, S. Marras, G. Bertoni, A. Guerfi, A. Vijh, M. Armand and K. Zaghib, *J. Mater. Chem. A*, 2017, **5**, 18919–18932.
31 J. Calbo, M. J. Golomb and A. Walsh, *J. Mater. Chem. A*, 2019, **7**, 16571–16597.
32 R. Konta, T. Ishii, H. Kato and A. Kudo, *J. Phys. Chem. B*, 2004, **108**, 8992–8995.
33 A. Kudo, K. Omori and H. Kato, *J. Am. Chem. Soc.*, 1999, **121**, 11459–11467.
34 K. Ogawa, O. Tomita, K. Takagi, A. Nakada, M. Higashi and R. Abe, *Chem. Lett.*, 2018, **47**, 985–988.
35 K. Chen, X. Chen and D. Xue, *CrystEngComm*, 2015, **17**, 1906–1910.
36 P. Refait and J. M. R. Génin, *Corrosion Science*, 1993, **34**, 797–819.
37 S. J. Clark, M. D. Segall, C. J. Pickard, P. J. Hasnip, M. I. J. Probert, K. Refson and M. C. Payne, *Z. Kristallogr.*, 2005, **220**, 567–57